Water Air Soil Pollut (2022) 233:152
https://doi.org/10.1007/s11270-022-05616-7

Softwood-derived Biochar as a Green Material for the Recovery of Environmental Media Contaminated with Potentially Toxic Elements

Maria Vittoria Pinna · Gian Paolo Lauro · Stefania Diquattro · Matteo Garau · Caterina Senette · Paola Castaldi · Giovanni Garau

Received: 7 January 2022 / Accepted: 6 April 2022

Abstract In this study, the effectiveness of softwood-derived biochar (BC) in the retention of potentially toxic elements (PTE, i.e., Cu(II), Pb(II), As(V), and Sb(V)) was evaluated at different pH values (4.5, 6.0, and 7.0), along with its capacity to alleviate PTE phytotoxicity. At all pH values, sorption and kinetic isotherms followed the trend: Pb(II) (e.g., ~0.56 mmol g^{-1} at pH 6.0) > Cu(II) (e.g., ~0.33 mmol g^{-1} at pH 6.0) > As(V) (e.g., ~0.29 mmol g^{-1} at pH 6.0) > Sb(V) (e.g. ~0.24 mmol g^{-1} at pH 6.0). Kinetic data strongly correlated with the pseudo-second-order kinetic equation; Langmuir and Freundlich isotherm models suggested monolayer sorption of Cu(II), Pb(II), and As(V) onto the BC surface and the interaction of Sb(V) with BC sites characterized by distinct sorption energy (i.e., multilayer sorption). Scanning electron microscopy (SEM) with energy-dispersive X-ray (EDX) analysis of PTE-saturated BC showed that Pb(II) was mainly associated with O, Sb(V) with Ca and Fe, while Cu(II) and As(V) with Fe and O. This suggested that hydroxyl and carboxyl functional groups, amorphous Fe oxy-hydroxides, as well as PTE precipitation with BC components were likely responsible for BC sorption capacity. Treatment of PTE-saturated BC with $Ca(NO_3)_2$ and a range of environmentally relevant organic acids indicated that 6–11% of PTE were loosely bound and easily exchangeable, while up to 60% could be mobilized by the organic acids. Hydroponic plant-growth experiments using triticale plants showed that BC stimulated plant growth in the presence of PTE and reduced their phytotoxicity.

Keywords Biochar · PTE · Sorption isotherms · PTE release · SEM–EDX analysis · Phytotoxicity

Supplementary Information The online version contains supplementary material available at https://doi.org/10.1007/s11270-022-05616-7.

M. V. Pinna · G. P. Lauro · S. Diquattro · M. Garau · C. Senette · P. Castaldi (✉) · G. Garau
Dipartimento di Agraria, University of Sassari, Viale Italia 39, 07100 Sassari, Italy
e-mail: castaldi@uniss.it

M. V. Pinna
e-mail: mavi@uniss.it

G. P. Lauro
e-mail: gplauro@uniss.it

S. Diquattro
e-mail: sdiquattro@uniss.it

M. Garau
e-mail: matteo_gp@libero.it

C. Senette
e-mail: senette@uniss.it

G. Garau
e-mail: ggarau@uniss.it

1 Introduction

Soil pollution by potentially toxic elements (PTE) due to anthropogenic (e.g., industrial, mining, and agricultural) activities is a worldwide concern because of their toxicity, persistence, and accumulation (Wang

Published online: 21 April 2022

et al., 2019). Potentially toxic elements, defined by the United States Environmental Protection Agency (USEPA) and the European Union as priority pollutants, can affect both soil physico-chemical properties and biochemical functioning (e.g., Castaldi et al., 2009). Moreover, they can have negative effects on plant growth and can be transferred into the human food chain, causing remarkable health risks (Antoniadis, Golia, et al., 2019). Some PTE, e.g., metal cations such as Cd and Pb, and oxyanionic metalloids such as As and Sb, can have remarkable toxic effects in the soil environment even when they are present in limited amounts (Antoniadis, Shaheen, et al., 2019).

Furthermore, although some PTE are considered essential (micro)nutrients for plants (e.g., Cu and Zn) and play a significant physiological role in plant metabolism, they can become toxic when certain thresholds are exceeded (Dal Corso, 2012).

In order to reduce the mobility and bioavailability of PTE in contaminated soils, or other environmental media, which is a primary aim of any environmentally friendly remediation interventions, appropriate solutions must be taken. Among the latter, isolation and containment, phytoremediation, and in situ chemical treatment are probably the most widely used (Palansooriya et al., 2020). In situ chemical immobilization of PTE using organic amendments constitutes an environmental-friendly approach which attracted particular attention in the last 25 years (Garau G. et al., 2021). In particular, soil treatment with biochar (BC) represents a green, sustainable, and climate-friendly promising remediation strategy for PTE-contaminated soils (Maiti & Ghosh, 2021). Biochar, a carbon-rich by-product obtained from the pyrolysis of different biomasses at high temperatures (e.g., 300–800 ℃) under the condition of limited oxygen, is rich in hydroxyl, ester, nitro, carboxyl, and carbonyl functional groups (Sohi et al., 2010) and is characterized by high pH, cation exchange capacity (CEC), and specific surface area (Mukome et al., 2013). Due to these features, BC could effectively stabilize (i.e., immobilize) PTE through precipitation, inner-sphere complexation, and ion exchange processes (Bandara et al., 2020), thereby reducing PTE bioavailability and uptake by plants, as well as the risk of their spread into the environment. Furthermore, BC addition to soil often increases the pH as well as P, Ca, and Mg availability and limits soil nutrient leaching, thus favoring plant growth in PTE-polluted areas (Garau G. et al., 2021; Manzano et al., 2020). However, BC immobilization efficiency is highly dependent on its physico-chemical properties (Assa Alber et al., 2021), which in turn are related to the type of biomasses used, their moisture and mineral content, and the process parameters applied, such as temperature, heating time, and oxygen availability (Evangelou et al., 2015; Pinna et al., 2020). The biomass properties mostly affect BC's total organic carbon and its mineral content, whereas BC surface area, porosity, pH, and recalcitrant carbon content are primarily influenced by treatment temperatures (Pinna et al., 2016; Zhao et al., 2013). For example, softwood-derived BC obtained at high temperature (e.g., 800 ℃) is commonly characterized by an alkaline pH, a porous structure encompassing micro, meso, and macro pores (Xu et al., 2017), and low mineral content (if compared to manure-derived BC; Manzano et al., 2020; Xu et al., 2017).

Previous studies on the effectiveness of BC in PTE retention highlighted that it also depends on the type of PTE. For instance, Namgay et al. (2010) observed increased concentrations of extractable As and Zn, decreased concentration of extractable Pb, and no effect on extractable Cu after the application to soil of wood biochar pyrolyzed at 550 ℃. Moreover, the addition of hardwood-derived biochar to a multi-element contaminated soil decreased the mobility of Zn and Cd, while increasing that of As and Cu (Beesley et al., 2010). Cd and Pb solubility in a contaminated paddy field was reduced by the incorporation of wheat straw BC (Bian et al., 2014). Up to 175-fold reduction of Cd, Pb, Cu, and Zn in pore water of a mine soil treated with BC, produced from residues of orchard prunings pyrolyzed at 500 ℃, was recorded by Beesley et al. (2014), which however reported an enhanced As mobility most probably due to the increased soil pH after BC addition. He et al. (2019), investigating the impact of kenaf core and sewage sludge BC on PTE immobilization, observed that both chars immobilized Pb and Cu, whereas they had little effect on Zn, Cd, and As. Finally, upon BC application to Pb and As co-contaminated soil, an increased As mobility and a significant reduction of labile Pb were observed (Abdelhafez et al., 2014).

Importantly, BC effectiveness in the recovery of PTE-polluted sites is also related to soil physico-chemical properties, as well as competitive sorption or desorption processes occurring in soil. All these latter, by determining PTE distribution between the

solid and liquid phase, ultimately regulate their bioavailability to plants or phytoavailability (Chen et al., 2018). In addition, the rhizosphere environment can have considerable effects on PTE bioavailability (Garau G. et al., 2019a; Garau M. et al., 2021). In particular, low molecular weight organic acids (e.g., citric, malic, and oxalic acids), which can be present at high concentrations in the rhizosphere (e.g., up to 80 mM; Adeleke et al., 2017), could significantly interfere with PTE mobility and bioavailability in the presence of BC (Adeleke et al., 2017). And the same applies to changes in pH due to root activities occurring in soil hotspots (Kuzyakov et al., 2015).

Overall, the heterogeneity and complexity of these aspects highlight the need for a deeper understanding of both BC-PTE interactions and the mechanisms involved in PTE immobilization/mobilization, as well as their possible relevance for plant growth and/or phytotoxicity. Accordingly, the aims of this study were (i) to assess the effectiveness of a softwood-derived BC in the sorption of selected PTE (i.e., Cu(II), Pb(II), As(V), and Sb(V)) from aqueous solution at different pH values, (ii) to examine the capacity of different organic acids commonly present in the rhizosphere (or in soil hotspots) to release the PTE adsorbed by BC, and (iii) to evaluate the BC potentials to alleviate PTE phytotoxicity.

2 Materials and Methods

2.1 Biochar Origin and Characterization

The studied BC was provided by Ronda SpA (Zanè, Italy) and was obtained by slow pyrolysis at 700 ℃ of beech, poplar, and elder (soft)wood. The BC pH and electric conductivity were measured on 1:5 (w/v) solid to water suspension (UNI EN 13,040, 2008). Total organic carbon (TOC) and total N were determined using a CHN analyzer (Leco CHN 628) with Oat meal Leco part n° 502–276 as a calibration sample; dissolved organic carbon (DOC) was determined using a 1:10 ratio (w/v) solid to water suspension (Silvetti et al., 2014). Cation exchange capacity (CEC) and the concentration of exchangeable Ca, K, and Mg were measured using the $BaCl_2$-triethanolamine method (Gazzetta Ufficiale, 1992). Extractable P was determined using the Olsen method (Olsen, 1954). Total and carboxylic acidity were determined through the $Ba(OH)_2$ and $Ca(OAc)_2$ methods, respectively (Schnitzer & Gupta, 1965). The quantity of phenolic OH was calculated by the difference between total acidity and COOH content. Total PTE concentration was quantified after BC digestion with HNO_3 and HCl (ratio 3:1 v/v) in a Microwave Milestone MLS1200 using a PerkinElmer AAnalyst 400-HGA 900 graphite furnace atomic absorption spectrometer (GF-AAS). A standard reference material (NIST-SRM 2711a) was included for quality assurance and quality control.

2.2 Preparation of Solutions

All reagents, if not differently specified, were obtained from Fluka (Fluka AG, Buchs, Switzerland) and solutions prepared by using deionized water (Milli-Q water; resistivity ≤ 18 MΩ cm); 2.0 mM $Pb(NO_3)_2$, $Cu(ClO_4)_2{\cdot}6H_2O$, $KSb(OH)_6{\cdot}7H_2O$, and $Na_2HAsO_4{\cdot}7H_2O$ solutions were employed as Pb(II), Cu(II), Sb(V), and As(V) sources, respectively. If needed, the pH of the BC/polluting solution systems was adjusted to 4.5, 6.0, and 7.0 with $HClO_4$ or NaOH solutions.

2.3 Sorption Kinetics of Pb(II), Cu(II), Sb(V), and As(V) by BC at Different pH Values

Sorption kinetics of Pb(II), Cu(II), Sb(V), and As(V) by BC at different pH values [i.e., 4.5 and 6.0 for Pb(II) and Cu(II), 4.5, 6.0, and 7.0 for Sb(V) and As(V)] were carried out by adding, to 0.1 g of BC, 100 mL of 2.0 mM PTE solutions brought to pH 4.5, 6.0, or 7.0. At pH 7.0 and at the concentration of Pb and Cu tested (i.e., 2 mM), the species $PbOH^+$ and $Pb(OH)_2^-$ and $CuOH^+$ and $Cu(OH)_2$ become dominant, resulting in the formation of Pb(II) and Cu(II) precipitates (Ford et al., 2007). For this reason, sorption kinetics of Pb(II) and Cu(II) by BC were performed at pH values of 4.5 and 6.0. The final mixtures were shaken at constant temperature (20 ± 1 ℃) for different times, i.e., 5 min, 10 min, 15 min, 30 min, 60 min, 120 min, 180 min, 360 min, 480 min (Fig. 1). At each time point, the samples were allowed to settle and filtered using 0.2 µm syringe filters. Supernatant aliquots were taken, and PTE in solution were quantified using a PerkinElmer AAnalyst 400-HGA 900 GF-AAS. Sorption kinetics were replicated in triplicate, and mean values ± standard deviations were reported. Kinetic datasets were processed using the following linearized equations

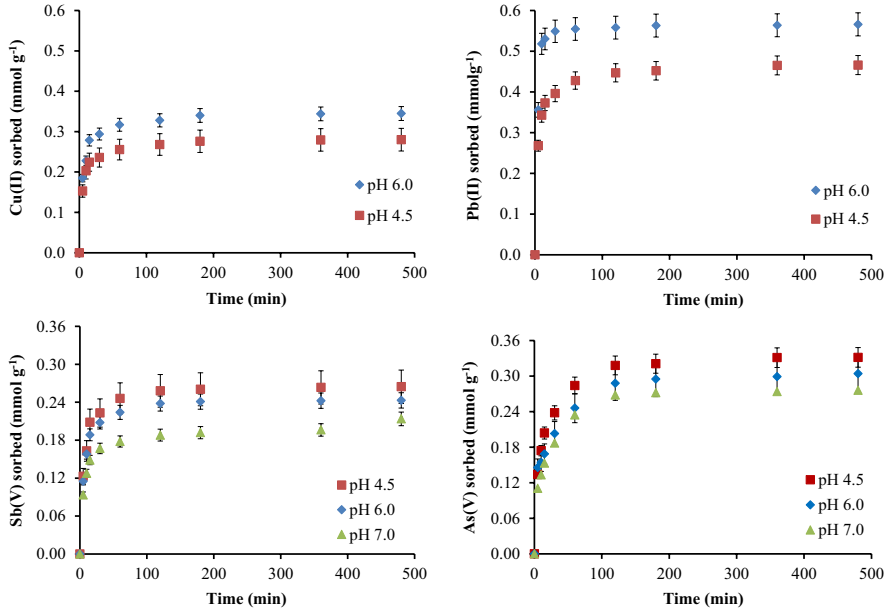

Fig. 1 Sorption kinetics of PTE by BC at different pH values

describing pseudo-first-order (PFO), pseudo-second-order (PSO), and Elovich kinetic models:

$$\log(qe - qt) = logqe - (\frac{k}{2.303})t \text{ (PFO)} \quad (1)$$

$$\frac{1}{qe-qt} = \frac{1}{qe} + kt \text{ (PSO)} \quad (2)$$

where qe is the amount of solute sorbed at equilibrium (mmol·g^{-1}), qt is the amount of solute sorbed at any time t (mmol·g^{-1}), and k is the rate constant of PFO (1·min^{-1}) and PSO sorption (mg·mmol $^{-1}$ min^{-1}, respectively).

$$qt = \left(\frac{1}{b}\right)\ln(ab) + (\frac{1}{b})lnt \text{ (Elovich)} \quad (3)$$

where qt is the amount of solute sorbed at any time t (mg·g^{-1}), a is the initial solute sorption rate (mg·g^{-1}·min^{-1}), and b is the Elovich constant (g·mg^{-1}). The coefficient of correlation (R^2) was used to estimate the fitness of experimental data to each model.

2.4 Sorption Isotherms of Pb(II), Cu(II), Sb(V), and As(V) on BC at Different pH Values

Biochar samples (0.1 g) were artificially and separately enriched with solutions (100 mL) containing increasing concentrations of Pb(II), Cu(II), Sb(V), and As(V) [brought to pH 4.5 and 6.0 for Pb(II) and Cu(II) and 4.5, 6.0, and 7.0 for As(V) and Sb(V)] to obtain sorption isotherms at different pH values. Nine different concentrations of Pb(II), Cu(II), As(V), and Sb(V), varying from 0.0 to 2.0 mM, were used to obtain the sorption isotherms (Fig. 2). The mixtures were shaken for 24 h at a constant temperature (20 ± 1 ℃). Afterward, the samples were allowed to settle and filtered, as previously mentioned. The PTE concentrations in the supernatant were determined as described above.

The sorption data were fitted to Langmuir and Freundlich models, and the corresponding relevant parameters were determined, i.e., b and K (Langmuir) and K_F and $1/n$ (Freundlich). The Langmuir equation, which is based on the assumption that the sorbent surface has a definite number of energetically equivalent sorption sites at which one chemical species may be adsorbed, is described by Eq. (4):

$$\frac{x}{m} = \frac{KbC}{1+KC} \text{ (Langmuir)} \quad (4)$$

where x/m is the sorbate amount adsorbed at equilibrium (mg·g^{-1}), b is the maximum monolayer coverage capacity of the sorbent (mg·g^{-1}), K (dm^3 mg^{-1}) is a constant related to the energy of sorption which quantitatively reflects the affinity between the sorbent and the sorbate, and C is the concentration of sorbate in the supernatant at equilibrium (mg L^{-1}).

The Freundlich equation is the most widely applied nonlinear sorption model and assumes that

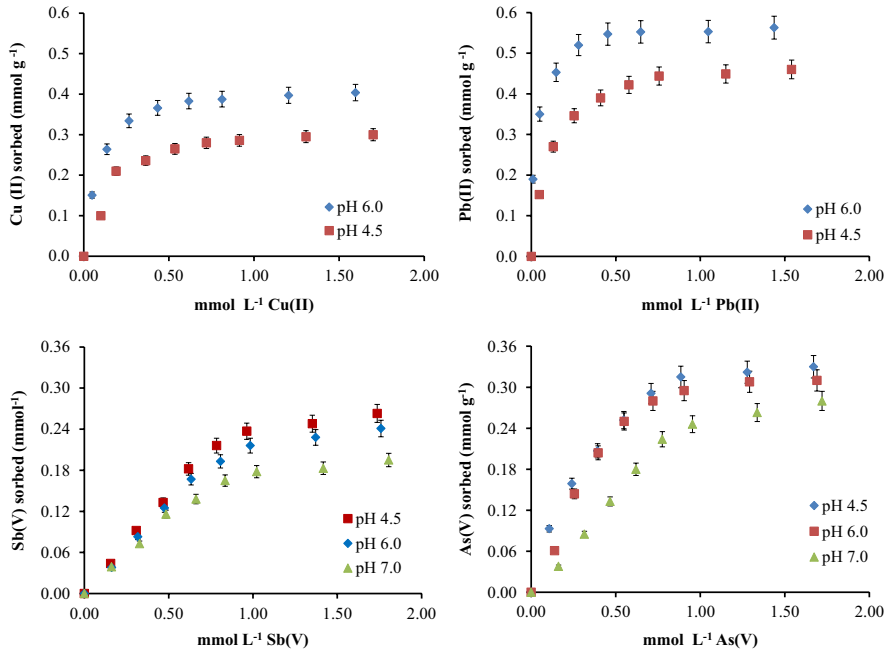

Fig. 2 Sorption isotherms of PTE by BC at different pH values

sorption can occur at energetically different heterogeneous surface sites. The Freundlich equation is depicted in Eq. (5):

$$\frac{x}{m} = K_F C^{1/n} \text{ (Freundlich)} \quad (5)$$

where K_F and n are the Freundlich equilibrium constant and exponent, respectively, which quantify sorbate uptake capacity (K_F) and intensity (n). The coefficient of correlation (R^2) was used to estimate the fitness of experimental data to the Langmuir and Freundlich models.

2.5 FT-IR Spectroscopy

Biochar FT-IR spectra (transmittance vs. wavenumber ν in the 370–4000 cm^{-1}) were collected in ATR mode using a Bruker Alpha Platinum-ATR interferometer (4 cm^{-1} resolution), as described in Piga et al. (2016). Each spectrum was obtained by averaging 256 interferograms.

2.6 Scanning Electron Microscopy and Energy-dispersive X-ray Spectroscopy Analysis

Scanning electron microscopy (SEM) and energy-dispersive X-ray spectroscopy (EDX) analyses of untreated BC and BC doped with PTE [i.e., saturated with 2.0 mM Cu(II), Pb(II), Sb(V), and As(V) solutions] at pH 4.5, 6.0, and 7.0 were carried out using an environmental scanning electron microscope ESEM-Zeiss EVO LS10 (Oberkochen-Germany). Biochar-PTE samples were observed with the backscattered electron detector (BSD) and chemically analyzed with a microanalysis X-ray energy-dispersive device (EDS) INCAx-ACT (Oxford Instruments). The whole process occurred at low vacuum mode and a pressure of 10 Pa.

2.7 Influence of Organic and Inorganic Anions on PTE Release by BC at Different pH Values

Potentially toxic elements-saturated BC at pH 4.5, 6.0, and 7.0 (i.e., those deriving from the last point of the sorption isotherms) were washed with distilled water and dipped into 100 mL of the following solutions (8 mM concentration) previously brought at the same pH of the respective BC-PTE systems: $Ca(NO_3)_2$, EDTA, and malic (MA), citric (CA), and oxalic (OA) acids. The solutions in contact with BC-PTE systems were shaken for 24 h at a constant temperature (20 ± 1 ℃), and then they were allowed to settle and filtered with 0.2-µm syringe filters. Potentially toxic elements in the solution

were quantified, as previously mentioned. At each pH value, mean concentrations of PTE released by the different treatments were analyzed by one-way analysis of variance (one-way ANOVA). When significant *P*-values were obtained (i.e., $P < 0.05$), differences between means were investigated using the post-hoc Fisher's least significant difference test ($P < 0.05$). Statistical analyses were carried out using the NCSS 2007 Data Analysis software (v. 07.1.21; Kaysville, Utah).

2.8 Influence of BC on PTE Phytotoxicity at Different pH Values

The influence of BC on PTE phytotoxicity was evaluated using triticale plants (×*Triticosecale* Wittm. cv. Universal) grown in polypropylene containers filled with aqueous solutions containing different PTE concentrations with or without BC as previously described (Garau G. et al., 2015). In particular, plant growth was assessed in aqueous systems (150 mL) brought at pH 4.5, 6.0, and 7.0 containing (i) 100 mg BC [BC]; (ii) 20 mM [PTE(1)], 100 mM [PTE(2)], and 200 mM [PTE(3)] PTE solutions; and (iii) BC + PTE(1) [PTE(1)-BC], BC + PTE(2) [PTE(2)-BC], and BC + PTE(3) [PTE(3)-BC]. Triticale seeds were germinated in the dark at 24 ℃ in cylindrical polystyrene containers (15 seeds per container) covered by a stainless-steel net and filled to the rim with 150 mL of 1 mM $CaCl_2$ solution. Five days after germination, germinated seeds were transferred (with the stainless-steel net) to the above-mentioned aqueous systems where triticale seedlings were grown under natural light for 7 days. At harvest, root and shoot length were measured, dried at 60 ℃ for 2 days, and then weighted. During the experiments, the containers were covered with foil to avoid root contact with light and photo-chemical reactions. Plant measurement data are presented as mean values ± standard errors.

The BC influence on the shoot and root growth in the presence of PTE was investigated by one-way ANOVA, and where significant *P*-values were obtained ($P < 0.05$), differences between individual means were compared using the post-hoc Fisher's least significance difference test (LSD, $P < 0.05$). Statistical analyses were carried out using the NCSS 2007 Data Analysis software (v. 07.1.21; Kaysville, Utah).

3 Results and Discussion

3.1 BC Chemical Properties

Biochar efficiency in the mitigation of environmental pollution due to PTE is primarily affected by its physico-chemical properties other than PTE type and pH of the medium, which influences both the surface charge of the adsorbent (i.e., BC) and PTE speciation.

The BC used in this study (Table 1) was characterized by a very alkaline pH (i.e., 9.3) and a total carbon content of ~ 61%, in line with values reported in the literature for chars obtained from softwood pyrolysis (Mukome et al., 2013). The low H/C molar ratio value (0.1) was indicative of high stability and aromaticity, as well as the presence of graphite-like structures (Stella Mary et al., 2016). This was confirmed by the FT-IR peak at ~ 1400 cm^{-1} assigned to C = C stretching within the aromatic ring (Fig. 3). The studied BC contained high concentrations of extractable P and exchangeable Ca, while PTE concentration was under the detection limit, except for Cu and Mn, whose concentration was, however, below the threshold limits imposed by the Italian legislation for amendments and fertilizers (MIPAAF, 2015). The substantial presence of phenolic groups (carboxylic ones were very limited; Table 1) can be deemed as promising for the fixation of cationic PTE as well as the complexation of anionic PTE. However, especially in the latter case, this should be experimentally tested and quantified since the loss of oxygenated functional groups which occurs at high pyrolysis temperature (i.e., our case) could significantly reduce BC sorption of anionic PTE such as As.

3.2 Sorption Kinetics of Pb(II), Cu(II), Sb(V), and As(V) by BC at Different pH Values

The kinetic isotherms of the different PTE, at different pH values, are presented in Fig. 1. The kinetic curves, which were clearly biphasic, showed fast initial sorption in the first 60 min, followed by a slower step, and the attainment of equilibrium after 120 min. The sorption of Pb(II) and Cu(II) was higher and faster at pH 6.0 than at pH 4.5 (indeed, after the first hour, more than 96% and 91% of Pb(II) and Cu(II) were adsorbed at pH 6.0, while ~ 90% was adsorbed at pH 4.5). Conversely, Sb(V) and As(V) sorption progressively reduced as the pH increased, i.e., by

Table 1 Selected BC chemical properties

Chemical analyses	
pH	9.30 ± 0.01
pH_{PZC}	5.0 ± 0.01
EC ($\mu S \cdot cm^{-1}$)	9.91 ± 2.79
Ash (%)	2.44 ± 0.10
Cation exchange capacity (CEC, $cmol_{(+)}\ kg^{-1}$)	18.81 ± 0.30
Total organic carbon (%)	61.32 ± 0.06
Total nitrogen (%)	0.30 ± 0.02
Total carbonate (%)	1.52 ± 0.02
Water dissolved organic carbon (DOC, $mg \cdot kg^{-1}$)	0.020 ± 0.003
Extractable P ($mg \cdot kg^{-1}$)	84.52 ± 3.01
Exchangeable K ($cmol_{(+)}\ kg^{-1}$)	0.62 ± 0.02
Exchangeable Ca ($cmol_{(+)}\ kg^{-1}$)	45.08 ± 0.95
Exchangeable Mg ($cmol_{(+)}\ kg^{-1}$)	3.28 ± 0.03
COOH groups ($meq \cdot g^{-1}$)	0.14 ± 0.02
Phenolic groups ($meq \cdot g^{-1}$)	2.10 ± 0.32
Totale Fe ($mg \cdot kg^{-1}$)	524.8 ± 12.7
Total PTEs concentration ($mg \cdot kg^{-1}$)	
Sb	n.d
As	n.d
Cd	n.d
Mn	358.1 ± 5.1
Pb	n.d
Cu	207.1 ± 2.9
Zn	n.d

d.wt., dry weight; *n.d.*, under detection limit (i.e., < 0.2 $\mu g \cdot L^{-1}$)
Values represent mean ± SE ($n = 3$)

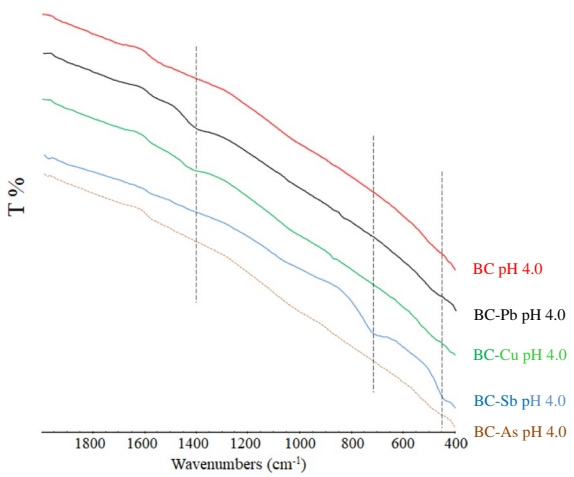

Fig. 3 FT-IR spectra of BC before and after PTE sorption at pH 4.0

28% and 18%, respectively, after the first hour when the pH changed from 4.5 to 7.0. The fast initial step, which concerned all PTE, was probably governed by a coulombic attraction between PTE ions in solution and charged functional groups on the BC surface, while the slower step was likely governed by chemisorption and/or precipitation reactions. In the case of cationic PTE, also cation-π interactions involving BC aromatic structures could have contributed to the fast initial step, while PTE intraparticle diffusion within BC meso and micropores could have contributed to the slower sorption kinetic step recorded for both cationic and anionic PTE.

Biochar-charged functional groups likely had a major role in PTE sorption, as highlighted by the different sorption behaviors of cationic and anionic PTE when varying the pH. In particular, the point of zero charge (pH_{PZC}) of BC is equal to 5.0, and at pH 4.5 (i.e., $pH < pH_{PZC}$), its surface should have a net positive charge which facilitates the sorption of negatively charged arsenate and antimonate anions [i.e., $H_2AsO_4^-$ and $Sb(OH)_6^-$], while an opposite trend should occur for Pb(II) and Cu(II) cations. When the pH rises above the pH_{PZC} (i.e., pH 6.0 and 7.0), the BC surface becomes predominantly negatively charged and oxyanions sorption is affected by Coulombic repulsion and competition with OH^- ions and other (inorganic and/or organic) anions for the same BC sorption sites. On the contrary, in these conditions (i.e., at increasing pH values), surface sorption of cationic PTE such as Pb(II) and Cu(II) is greatly facilitated.

Different kinetic models were used in this study to describe the sorption of PTE by a solid adsorbent, i.e., the pseudo-first-order, pseudo-second-order, and Elovich kinetic models. The pseudo-second-order model better described the experimental data (R^2 ranging from 0.999 to 1.000, Table 2) for all the PTE analyzed, suggesting chemisorption as the rate-limiting step of the sorption process (Robati, 2013). According to Ho and McKay (2000), the chemisorption of cationic PTE probably involved the sharing or exchange of electrons between BC functional groups (e.g., phenolate, carboxylate) and divalent metal cations, as well as inner-sphere complexation between anionic PTE and bonding groups on BC surfaces (e.g., hydroxyl, carboxyl, and C-O ester of alcohols).

Based on the results of the kinetic isotherms and data fitting to kinetic models, the following

Table 2 Kinetic model parameters for the metal adsorption on BC at different pH values

	Pseudo-first-order equation		Pseudo-second-order equation		Elovich equation		
	$\log(qe-qt)=logqe-\left(\frac{k}{2.303}\right)t$		$\frac{1}{qe-qt}=\frac{1}{qe}+kt$		$qt=\left(\frac{1}{b}\right)\ln(ab)+(\frac{1}{b})lnt$		
	k	R^2	k	R^2	a	b	R^2
pH 4.5							
Cu(II)	$6.91{\cdot}10^{-4}$	0.398	0.775	1.000	11.932	16.722	0.875
Pb(II)	$6.91{\cdot}10^{-4}$	0.456	0.390	0.999	42.985	10.881	0.907
Sb(V)	$9.21{\cdot}10^{-4}$	0.332	0.873	0.999	2.855	15.221	0.814
As(V)	$1.38{\cdot}10^{-3}$	0.482	0.298	0.999	0.533	9.497	0.945
pH 6.0							
Cu(II)	$6.91{\cdot}10^{-4}$	0.427	0.506	0.999	13.742	13.550	0.882
Pb(II)	$4.61{\cdot}10^{-4}$	0.188	0.925	0.999	$5.2{\cdot}10^{4}$	14.771	0.532
Sb(V)	$9.21{\cdot}10^{-4}$	0.362	0.957	0.999	5.017	17.889	0.845
As(V)	$1.38{\cdot}10^{-3}$	0.565	0.315	0.999	0.580	10.846	0.937
pH 7.0							
Sb(V)	$9.21{\cdot}10^{-4}$	0.431	0.518	0.999	1.670	19.378	0.894
As(V)	$1.61{\cdot}10^{-3}$	0.515	0.301	0.999	0.306	10.707	0.945

q_e and q_t (mmol g^{-1}) are the adsorption capacities at equilibrium and time t (min), respectively; k (mmol g^{-1} min^{-1}) is the rate constant; a is the initial adsorption rate (mmol g^{-1} min^{-1}), and b is related to the extent of surface coverage and the activation energy involved in chemisorption (g mg^{-1})

hypotheses can be done to explain the mechanisms underpinning Pb(II) and Cu(II) sorption by BC: (i) electrostatic outer sphere (non-specific) complexation due to metal exchange with Ca^{2+}, K^+, and Na^+ present in BC (this is expected to govern the first phase of the kinetic curve); (ii) inner-sphere (specific) complexation (or chemisorption), as well as intraparticle diffusion and/or Pb(II) and Cu(II) precipitation with some BC inorganic components, e.g., oxy-hydroxides, carbonates, and phosphates, to form insoluble compounds (these processes are expected to govern the second step of the kinetic curve). Similar hypotheses can be done to explain the mechanisms of As(V) and Sb(V) sorption by BC: (i) non-specific Sb(V)/As(V) binding to anion-exchange sites on BC surfaces (e.g., protonated amino groups), or to (coordinating) metal cations within BC [e.g., Mg(II) and Ca(II)] where such metals act as bridging elements between Sb(V) or As(V) and other negatively charged functional groups within BC surfaces (e.g., carboxylic and phenolic groups) (this is expected to govern the first phase of the kinetic curve); (ii) inner-sphere (specific) complexation (or chemisorption) of Sb(V) and As(V) with Fe-(hydr)oxides physically and/or chemically bound to the organic BC components (Table 1), intraparticle diffusion and/or Sb(V) and As(V) precipitation with some BC inorganic components, e.g., Ca(II) which was abundantly present in BC, to form insoluble compounds (these processes are expected to govern the second step of the kinetic curve).

3.3 Sorption Isotherms of Pb(II), Cu(II), Sb(V), and As(V) on BC at Different pH Values

To further investigate the sorption mechanisms and interaction types between BC and PTE, sorption isotherms were obtained at pH 4.5 and 6.0 for Pb(II) and Cu(II), and also at pH 7.0 for As(V) and Sb(V) (Fig. 2). The BC sorption capacities, determined on the basis of the maximal experimental amount of PTE sorbed at equilibrium, were 0.30 mmol g^{-1} BC and 0.40 mmol g^{-1} BC for Cu(II) and 0.45 mmol g^{-1} BC and 0.55 mmol g^{-1} BC for Pb(II) at pH 4.5 and 6.0, respectively. The observed increase in Cu(II) and Pb(II) sorption at the higher pH is due to a decreased competition between protons and metal cations for the same BC functional groups and to a reduction of positively charged sites on the BC surface ($pH_{PZC}=5.0$) which lowered the electrostatic repulsion between BC and Cu(II) and Pb(II). The higher sorption capacity

for Pb(II) could be attributed to its higher electronegativity constant compared to Cu(II) (2.33 *vs.* 1.90). This commonly results in a higher tendency of Pb(II) for specific sorption by the BC surface functional groups (e.g., –COOH and –OH) (Uchimiya et al., 2011). Sorption capacities of 0.26 mmol g^{-1} BC, 0.24 mmol g^{-1} BC, 0.19 mmol g^{-1} BC, and 0.33, 0.31, 0.28 mmol g^{-1} BC were determined for Sb(V) and As(V) at pH 4.5, 6.0, and 7.0, respectively. Given the substantial Fe content of BC (Table 1), Fe-(hydr) oxides were likely responsible for anion sorption (e.g., through specific and non-specific sorption processes), as previously pointed out (Agrafioti et al., 2014). The sorption of such anionic species decreased as the pH value raised from 4.5 to 7.0, and the maximum amount of Sb(V) sorbed by BC at pH 4.5 was about 1.4 times than that sorbed at pH 7.0. The influence of pH was less pronounced for As(V), for which the maximum amount sorbed at lower pH was about 1.2 times higher than that sorbed at pH 7.0. Moreover, a lower affinity of biochar for antimonate was detected compared to arsenate (Fig. 2). These results agree with Zhang et al. (2016), which observed a limited pH impact on As(V) sorption by a BC from hyacinth (up to pH values ~ 10), and higher sorption of As(V) compared to Sb(V). This was likely due to the fact that, at higher pH values, As(V) sorption (much more than Sb(V)) was mainly governed by chemical processes (i.e., formation of monodentate, mononuclear, and binuclear complexes with Fe–(hydr)oxides within BC). As previously highlighted, in the 6.0–7.0 pH range, arsenate anions are partially protonated, i.e., they retain one or two neutral hydroxyl groups ($pK_{a2} = 6.96$ and $pK_{a3} = 11.49$ for H_3AsO_4) that can be involved in the protonation of surface Fe–OH groups within BC facilitating ligand exchange reactions (Garau G. et al., 2019b). This is not possible for Sb(V), whose stable form at pH > 4 is the antimonate ion $Sb(OH)_6^-$, i.e., no deprotonation is expected.

The PTE sorption data were analyzed using the Langmuir and Freundlich isotherm models (Table 3). The sorption data for Cu(II), Pb(II), and As(V) at pH 4.5 and 6.0 fitted with the Langmuir sorption model, suggesting PTE monolayer sorption onto a BC surface with a finite number of identical sites. The correlation coefficient values ranged between 0.918 and 1.000, whereas for the Freundlich model, they ranged from 0.780 to 0.845. On the contrary, the Freundlich model better explained Sb(V) sorption at pH 4.5 and 6.0 and As(V) sorption at pH 7.0 (Table 3), suggesting that sorption likely occurred at energetically different BC surface sites.

Taken together, the results indicate that the PTE sorption capacity is pH-dependent and that BC has a greater Pb(II) sorption capacity compared to Cu(II), Sb(V), and As(V).

Table 3 The Langmuir and Freundlich parameters for the metal adsorption on BC at different pH values

	Langmuir parameters			Freundlich parameters		
	b (mmol g^{-1})	K ($Lmmol^{-1}$)	R^2	K_F (mmol g^{-1})	$1/n$	R^2
pH 4.5						
Cu(II)	0.332	6.724	0.995	0.295	0.337	0.780
Pb(II)	0.492	9.647	1.000	0.466	0.309	0.900
Sb(V)	0.485	0.810	0.858	0.219	0.757	0.932
As(V)	0.409	2.894	0.992	0.306	0.476	0.941
pH 6.0						
Cu(II)	0.424	12.957	1.000	0.410	0.267	0.861
Pb(II)	0.573	34.767	1.000	0.607	0.222	0.886
Sb(V)	0.461	0.732	0.820	0.197	0.197	0.925
As(V)	0.436	1.864	0.918	0.295	0.616	0.845
pH 7.0						
Sb(V)	0.311	1.084	0.929	0.161	0.679	0.927
As(V)	0.696	0.472	0.618	0.229	0.863	0.932

b is the maximum monolayer coverage capacity of the sorbent; K is a constant related to the energy of sorption; K_F and n quantify sorbate uptake capacity (K_F) and intensity (n)

3.4 FT-IR Analysis

In different studies, it was shown that the abundance of BC functional groups progressively reduced as pyrolysis temperature increased and this is clearly reflected by FT-IR spectra which lose complexity, especially for BCs obtained at high temperatures (e.g., Janu et al., 2021; Rodríguez-Vila et al., 2018). Apparently, this also applied to our case where BC was obtained at 700 ℃. In more detail, FT-IR spectra of BC after PTE sorption were characterized by few peak shifts which however can provide some indications on the PTE sorption mechanisms (Fig. 3). In particular, the band at ~ 1400 cm^{-1}, which can be ascribed to phenols (Silverstein et al., 1981), clearly increased in intensity for Pb- (especially) and Cu-saturated BC (Fig. 3), suggesting a possible interaction of this functional group with cationic PTE. Similar findings (and peak shifts) were reported by Soria et al. (2020) for different plant-derived BCs when saturated with Pb, Cd, and Zn. However, this band could also be due to the formation of Pb or Cu precipitates on the BC surface, such as hydrocerussite $Pb_3(CO_3)_2(OH)_2$ (e.g., Shen et al., 2020) or azurite $Cu_3(CO_3)_2(OH)_2$ (e.g., Ippolito et al., 2012), which are characterized by an intense peak at ~ 1400 cm^{-1} due to C–O stretching vibrations of CO_3^{2-} anions. No apparent differences were noted in this spectral region in untreated BC and in As- and Sb-saturated ones (Fig. 3). An intense band centered at ~ 700 cm^{-1} and another one centered at ~ 450 cm^{-1}, which could be ascribed to Sb–O stretching vibration (Liu et al., 2015), appeared in Sb-saturated BC, possibly suggesting Sb(V) immobilization by BC in the form of solid precipitates, e.g., calcium antimonate $Ca(Sb(OH)_6)_2$, while no apparent peak shift was recorded for As-saturated BC.

3.5 SEM–EDX Analysis of BC-PTE Systems

Scanning electron microscopy images at varying magnifications (~ 500–5000X) and EDX spectra of BC-PTE systems were recorded, and results of BC saturated with Pb(II) and Cu(II) at pH 4.5, and Sb(V) and As(V) at pH 7.0 are reported in Fig. 4 and in Supplementary Figs. S1 and S2, since those relative to the other pH values were very similar. With the exception of small amounts of Cu (i.e., 0.17%), PTE were not present in EDX spectra of untreated BC, while they were consistently detected in those related to PTE-saturated BCs (Fig. 4 and Supplementary Fig. S1). The EDX quantitative analysis thus supported PTE sorption by BC and revealed that O was the most

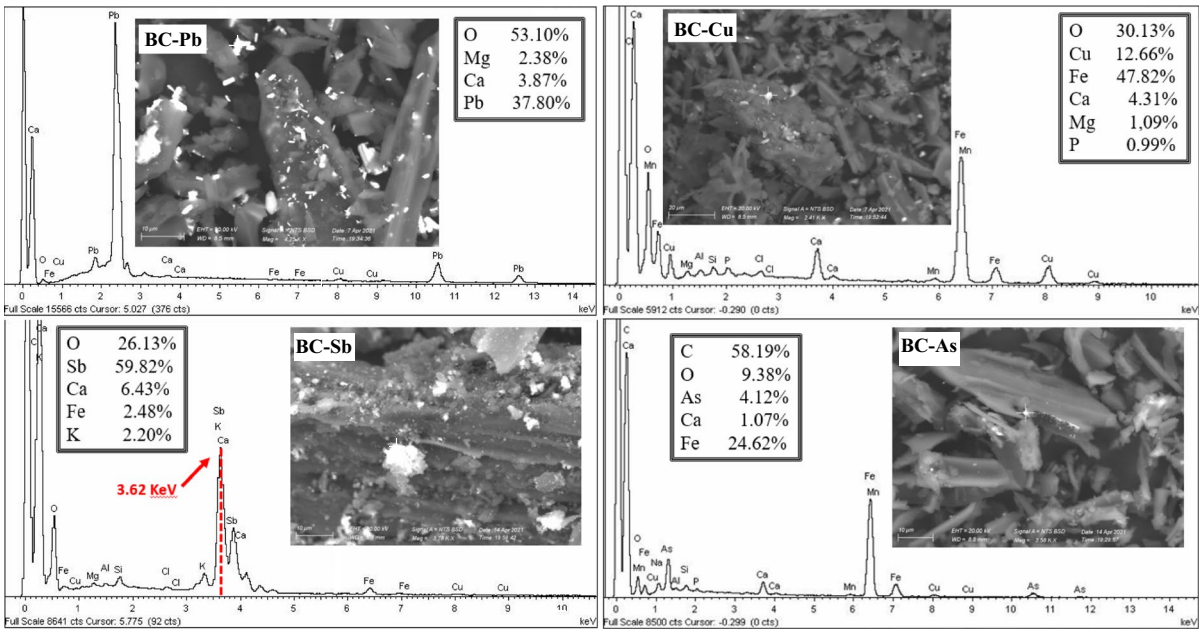

Fig. 4 SEM images and EDX spectra and elemental composition relative to different spot analyses of PTE-saturated BC. SEM magnification (×1000): BC-Pb, 4.25; BC-Cu, 2.41; BC-Sb, 3.78; BC-As, 3.68

abundant element in BC after C (~20% in untreated BC; Supplementary Fig. S1). Moreover, Fe, Ca, Mg, Cu, and Si were also revealed in limited amounts in untreated BC (Supplementary Fig. S1).

Backscattered electron images of BC-Pb and BC-Sb systems indicated a diffuse superficial distribution of these PTE which were present as bright and discrete precipitates (Fig. 4 and Supplementary Fig. S2). Moreover, SEM–EDX spot analysis indicated that Pb(II) was mainly associated with O, supporting the view that O-containing functional groups have an important role in Pb(II) immobilization (Fig. 4; Uchimiya et al., 2011). In this case, the formation of $Pb(OH)_2$ and/or PbO solid phases could be hypothesized as an important mechanism of Pb(II) fixation by BC which nevertheless does not exclude the involvement of outer and inner-sphere complexation, e.g., by carboxyl and or phenolic functional groups. SEM–EDX spot analysis also indicated that Sb(V) was associated with Ca and Fe possibly, suggesting (i) a substantial superficial coprecipitation of Sb(V) with Ca(II) and (ii) a more limited Sb(V) immobilization (e.g., inner-sphere complexation) by Fe (hydr)oxides within BC. Importantly, the energy peak at 3.62 keV (Fig. 4), due to the combination of Sb-Lα (3.605 keV) and Ca-Kα (3.691 V) emissions, supported the association of Sb(V) and Ca(II) in surface precipitates (Diquattro et al., 2018).

Backscattered electron images suggested a more limited presence of Cu(II) and As(V) on the BC surface (Fig. 4 and Supplementary Fig. S2), probably as a result of their preferential fixation within BC pores. This also suggests a reduced tendency of Cu(II) and As(V), compared to Pb(II) and Sb(V), to form insoluble precipitates. SEM–EDX spot analysis showed that Cu(II) and As(V) were mainly associated with Fe and O (Fig. 4). This supported the view that Cu(II) and As(V) sorption by BC mainly occurred through the formation of Fe–O–As(Cu) bonds and confirmed the high affinity of As(V) for Fe (hydr)oxides (Wilson et al., 2010). However, partial Cu(II) precipitation as (hydr)oxide could not be ruled out, as well as the involvement of BC functional groups in the formation of ternary complexes with Ca(II) and As(V).

3.6 Influence of Organic and Inorganic Anions on PTE Release by BC at Different pH Values

In the rhizosphere environment, the mobility and bioavailability of PTE sorbed by BC can be affected by root-induced changes in pH, as well as by the substantial presence of inorganic ions and low molecular weight organic acids (LMWOAs), e.g., citric, malic, and oxalic acids. In particular, these latter organic acids can form soluble metal–organic complexes with Cu(II) and Pb(II) sorbed by BC (Takeda et al., 2009) as well as with Ca(II) and Fe(III) possibly involved in Sb(V) and As(V) fixation. This can lead to an obvious increase in PTE mobility and potential bioavailability. Moreover, at $pH \geq 4.5$, where citric, malic, and oxalic acids are expected to be in anionic form, they can compete with Sb(V) and As(V) for the same BC sorption sites, thus interfering with possible Sb(V) and As(V) sorption by BC.

Therefore, to better investigate such aspects, the ability of $Ca(NO_3)_2$ and of citric (CA, $pK_{a1}=3.13$, $pK_{a2}=4.76$, $pK_{a3}=6.34$), malic (MA, $pK_{a1}=3.46$, $pK_{a2}=5.10$), and oxalic (OA, $pK_{a1}=1.25$, $pK_{a2}=3.81$) acids to mobilize the PTE sorbed by BC was evaluated at pH 4.5, 6.0, and 7.0. Ethylenediaminetetraacetic acid (EDTA), a very efficient chelating agent useful to predict potential bioavailability (and in risk assessment), was also used for comparison (Santos et al., 2010). The results obtained highlighted the different capabilities of $Ca(NO_3)_2$ and organic anions to mobilize PTE adsorbed by BC, being the inorganic salt the least effective at all pH values considered (Fig. 5). This suggests substantial stability of the interactions between BC and PTE. For instance, 12% and 17% of Cu(II) and 8% and 5% of Pb(II) were mobilized by PTE-saturated BC using $Ca(NO_3)_2$ at pH 4.5 and 6.0, respectively. This indicates both the shortage of labile and potentially bioavailable (i.e., exchangeable) Cu(II) and Pb(II) fractions (and the limited extent of weak interactions, e.g., π-metals binding) and the ability of these PTE to establish strong interactions with BC surfaces and/or its mineral components. This was also highlighted by the significant amount of Cu(II) and Pb(II) mobilized by EDTA and representing the relatively immobile and not readily bioavailable or leachable metal fraction (Basta & Gradwohl, 2000), i.e., 28% and 56% Cu(II) and 40% and 56% Pb(II) at pH 4.5 and 6.0, respectively (Fig. 5). Among LMWOAs, OA was the most effective in the mobilization of cationic PTE, whereas CA and OA significantly affected As(V) and Sb(V) release, i.e., more than MA (Fig. 5). Regarding Cu(II) and Pb(II), the greater stability of the 5-membered chelate complex that forms between the oxalate anion and these PTE (i.e., 1,4-bidentate chelation) could justify the highest amount of metal released after OA addition (47% and 50% at pH 4.5 and 74% and 56% at pH 6.0, for Cu(II) and Pb(II),

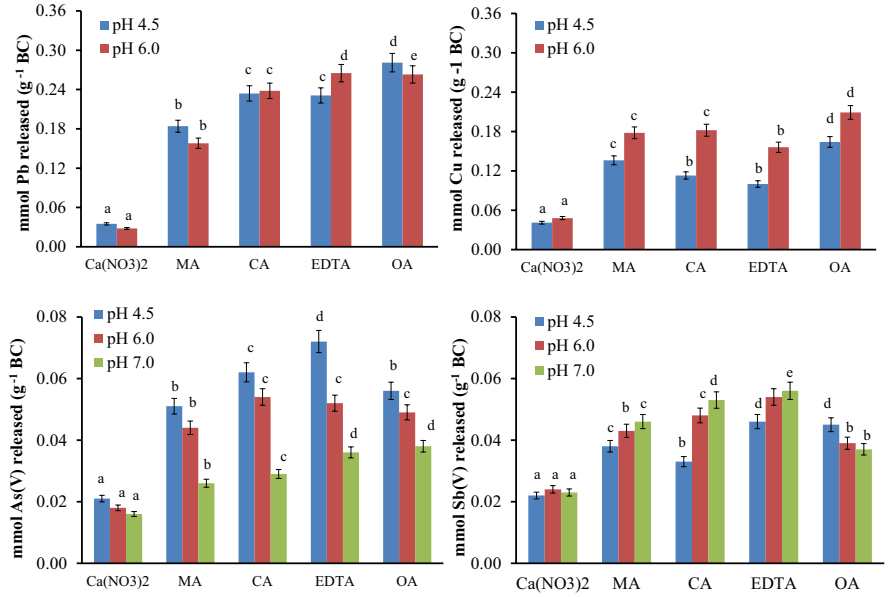

Fig. 5 PTE released from the BC-PTE systems after different treatments. For each pH value, mean values followed by different letters denote statistically significant differences according to Fisher's LSD test ($P < 0.05$)

respectively) than that mobilized by CA and MA. CA mobilized a higher amount of Pb(II) with respect to MA (Fig. 5), likely because of the higher stability constants of Pb-citrate complexes compared to Pb-malate (Silvetti et al., 2017).

Potentially bioavailable Sb(V) and As(V) fractions (i.e., extracted with $Ca(NO_3)_2$) were rather limited at all the pH values tested, being ~ 6% and 10% for As(V) and Sb(V), respectively (Fig. 5). As for cationic PTE, this indicates stable fixation mechanisms and substantial BC versatility in the retention of PTE in cationic and anionic form. Sb(V) and As(V) amounts released with EDTA solutions were more limited compared to Cu(II) and Pb(II), varying between 22 and 13% for As and 18% and 27% for Sb(V) (at pH 4.5 and 7.0, respectively). As a consequence, the majority of Sb(V) and As(V) retained by BC was hardly releasable and/or inaccessible and this can have obvious positive implications for environmental remediation strategies (Abou Jaoude et al., 2020; Manzano et al., 2020).

In the presence of LMWOAs, the released amounts of anionic PTE ranged from 13 to 28% and from 9 to 19% for Sb(V) and As(V), respectively. CA was the most efficient, releasing ~ 13%, 20%, and 28% and the 19%, 17%, and 10% of total Sb(V) and As(V) sorbed at pH 4.5, 6.0, and 7.0, respectively (Fig. 5). The formation of stable CA–Sb(V) complexes involving the hydroxyl and carboxyl groups of CA in the formation of two Sb–O–C bonds (Tella & Pokrovski, 2012) and the citrate-induced mineral dissolution of the Fe-phases involved in As(V) retention (Mohapatra et al., 2005) can explain the higher efficiency of citrate with respect to the other LMWOAs considered. The results obtained also showed that the PTE mobilization by the organic anions was pH-dependent, with lower percentages of Sb(V) and As(V) released at lower and higher pH, respectively. These findings agree with previous studies which showed higher release of Sb(V) at alkaline or neutral pH (e.g., Herath et al., 2017), while the maximum release of As(V) was observed at pH ~ 5.0–6.0 (Amarathunga et al., 2019; Mohapatra et al., 2005).

Overall, the results obtained indicated that LMWOAs common in soil hotspots and rhizosphere can mobilize different amounts of PTE sorbed by BC through both the formation of soluble PTE – ligand complexes and/or the dissolution of solid phases involved in PTE retention.

3.7 Influence of BC on PTE Phytotoxicity at Different pH Values

To assess the effectiveness of BC in alleviating Cu(II), Pb(II), Sb(V), and As(V) phytotoxicity, a series of experiments were carried out using triticale plants. The phytotoxicity of PTE was evaluated on plants grown in aqueous systems, brought at pH 4.5, 6.0, and 7.0, containing BC, PTE at different

concentrations (i.e., 20 mM, 100 mM, and 200 mM) and BC + PTE (20 mM, 100 mM, and 200 mM), and it was quantified by recording root and shoot length and the respective dry weight. Since the BC impact on PTE phytotoxicity was the same across the different pH values tested, only data related to plant growth at pH 6.0 were reported (Figs. 6 and 7).

Overall, a positive impact of BC on plant growth in the presence of PTE was observed. For instance, in the BC-Cu system, root length was 2.6-, 3.3-, and 3.1-fold higher in BC-Cu(1), BC-Cu(2), and BC-Cu(3), respectively, with respect to systems containing only Cu(II), and a similar trend was recorded in BC-Pb system (Fig. 6). The presence of BC also alleviated Sb(V) phytotoxicity, and this was particularly evident at the highest PTE concentrations (e.g., an increase of + 3.85 and 1.7-fold was detected in roots and shoots weight of plants grown in Sb(3)-BC with respect to Sb(3)). Although less pronounced, the effect of BC was similar in reducing As(V) phytotoxicity (Fig. 7). In particular, an increase of 1.7-, 1.3-, 1.9-, and 1.5-fold in root and shoot length, and root and shoot dry weight, respectively, was observed in BC-As(3) systems compared to As(3). Overall, these results clearly indicate that the studied BC can alleviate PTE phytotoxicity and possibly promote plant growth in polluted environments. This is consistent with recent studies by Kamran et al. (2020) and Wu et al. (2020) which reported significant biomass increases of rapeseed (*Brassica napus* L.) and *Vetiveria zizanioides* (L.) Nash species grown in Cu(II) and Pb(II) polluted soils amended with woodchip and Enteromorpha prolifera biochar, respectively. Similar findings were also reported by Mohamed et al. (2017) which observed reduced phytotoxicity of Pb, Co, and Ni toward wheat seedlings when switchgrass biochar was added to contaminated sandy soil. Overall, the results obtained suggest that the softwood biochar used was able to reduce the toxic effects of anionic and cationic PTE, probably due to a decrease in their labile fractions (readily soluble and/or exchangeable), thus supporting the chemical data.

4 Conclusions

The use of biochar in the remediation of PTE-contaminated soils, because of the heterogeneity of literature data regarding the PTE mobility and bioavailability, requires a deeper knowledge of the mechanisms and interaction types occurring between the sorbent (biochar) and the sorbate (PTE). The results obtained in this study provided additional insights as regards this issue. Sorption data are strongly correlated with the pseudo-second-order kinetic equation and together with the Langmuir sorption isotherm (except for Sb(V)), suggesting that the PTE sorption by BC is a complex phenomenon and probably a combination of different

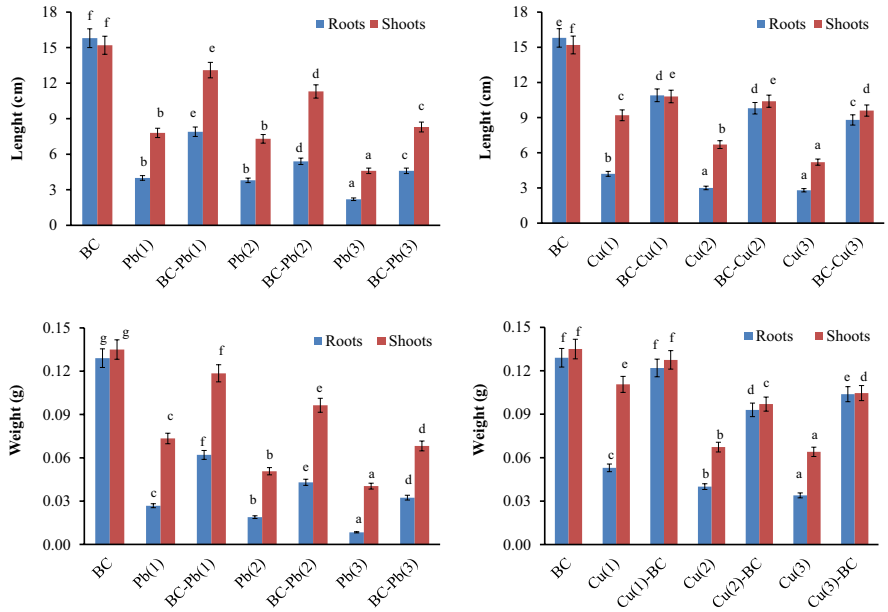

Fig. 6 Roots and shoot length and weight of triticale plants grown in different BC-Cu(II)/Pb(II) systems at pH 6.0. For each plant part, mean values followed by different letters denote statistically significant differences according to Fisher's LSD test ($P < 0.05$)

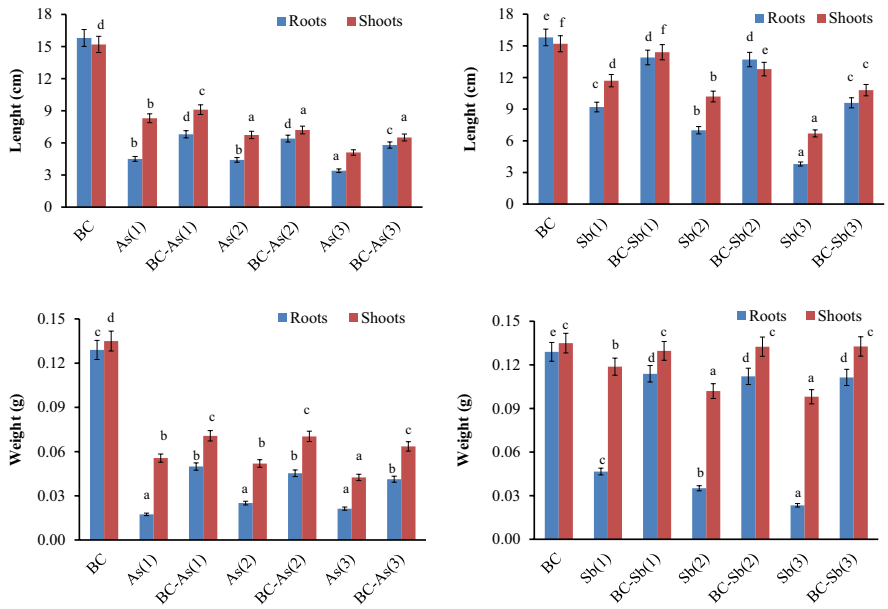

Fig. 7 Roots and shoot length and weight of triticale plants grown in different BC-As(V)/Sb(V) systems at pH 6.0. For each plant part, mean values followed by different letters denote statistically significant differences according to Fisher's LSD test ($P < 0.05$)

sorption mechanisms. The BC effectiveness in the PTE retention is pH-dependent and proportional to the available sites on the BC surfaces. Hydroxyl and carboxyl functional groups through the formation of inner-sphere complexes as well as amorphous Fe oxy-hydroxides within the biochar are responsible for BC sorption capacity. Due to Pb(II) high electronegativity constant as well as to its high affinity for –COOH and –OH functional groups above all (given the high concentration found in biochar), BC shows a greater Pb(II) retention compared to Cu(II), Sb(V), and As(V). In addition, some precipitation of Pb(II) as (hydr)oxide and Sb(V) with the calcium present in the biochar could be quantitatively important, as revealed by the SEM–EDX spectra. The sorption capacity of BC decreased the mobility or potential bioavailability of PTE. However, in the rhizosphere, a certain PTE mobilization can occur by the formation of soluble metal–ligand complexes with the organic anions present there (e.g., oxalate, citrate, and malate anions) or the dissolution of the phases involved in the retention. Finally, BC, as well as having a positive effect on plant growth, was able to effectively reduce the toxic effects of all the PTE studied.

The findings obtained can help to better understand the effectiveness of biochar in remediation programs of PTE-contaminated soils, and they can contribute to the knowledge of the mechanisms governing the interactions between different PTE (e.g., PTE in cationic and anionic form) and biochar.

Acknowledgements The financial support of the University of Sassari (Fondo di Ateneo per la Ricerca 2020) and the "Bando competitivo Fondazione di Sardegna – 2017 per progetti di ricerca con revisione tra pari" is gratefully acknowledged.

Dott. Crivello and the Company Ronda Engineering Srl (Zanè, Italy) are acknowledged for providing the biochar.

Author Contribution Maria Vittoria Pinna: investigation, methodology, formal analysis, writing – original draft preparation. Gian Paolo Lauro: formal analysis. Stefania Diquattro: methodology, formal analysis. Matteo Garau: methodology, formal analysis. Caterina Senette: investigation. Paola Castaldi: conceptualization, methodology, resources, writing – reviewing and editing. Giovanni Garau: conceptualization, methodology, writing – reviewing and editing.

Funding This work was supported by the University of Sassari (Fondo di Ateneo per la Ricerca 2020). Additional funding was provided by the "Bando competitivo Fondazione di Sardegna – 2017 per progetti di ricerca con revisione tra pari."

Data Availability The authors declare that all relevant data supporting the findings of this study are included in this article and its supplementary information files.

Declarations

Ethics Approval and Consent to Participate This work did not report on or involved the use of any animal or human data or tissue.

Consent for Publication This work did not contain data from any individual person.

Competing Interests The authors declare no competing interests.

References

Abdelhafez, A. A., Li, J., & Abbas, M. H. (2014). Feasibility of biochar manufacturated from organic wastes on the stabilization of heavy metals in a metal smelter contaminated soil. *Chemosphere, 117*, 66–71.

Abou Jaoude, L., Castaldi, P., Nassif, N., Pinna, M. V., & Garau, G. (2020). Biochar and compost as gentle remediation options for the recovery of trace elements-contaminated soils. *Science of the Total Environment, 711*, 134511–134520.

Adeleke, R., Nwangburuka, C., & Oboirien, B. (2017). Origins, roles and fate of organic acids in soils: A review. *South African Journal of Botany, 108*, 393–406.

Agrafioti, E., Kalderis, D., & Diamadopoulos, E. (2014). Arsenic and chromium removal from water using biochars derived from rice husk, organic solid wastes and sewage sludge. *Journal of Environmental Management, 133*, 309–314.

Amarathunga, U., Diyabalanage, S., Bandara, U. G. C., & Chandrajith, R. (2019). Environmental factors controlling arsenic mobilization from sandy shallow coastal aquifer sediments in the Mannar Island, Sri Lanka. *Applied Geochemistry, 100*, 152–159.

Antoniadis, V., Golia, E. E., Liu, Y., Wang, S., Shaheen, S. M., & Rinklebe, J. (2019a). Soil and maize contamination by trace elements and associated health risk assessment in the industrial area of Volos, Greece. *Environment International, 124*, 79–88.

Antoniadis, V., Shaheen, S. M., Levizou, E., Shahid, M., Niazi, N. B., Vithanage, M., Ok, Y. S., Bolan, N., & Rinklebe, J. (2019b). A critical prospective analysis of the potential toxicity of trace element regulation limits in soils worldwide: Are they protective concerning health risk assessment? A review. *Environment International, 127*, 819–847.

Assa Alber, H., Li, H., Jeyakumar, P., Wei, L., Huang, L., Huang, Q., Kamran, M., Shaheen, S. M., Hou, D., Rinklebe, J., Liu, Z., & Wang, H. (2021). Influence of biochar and soil properties on soil and plant tissue concentrations of Cd and Pb: A meta-analysis. *Science of the Total Environment, 755*, 142582–142593.

Bandara, T., Franks, A., Xu, J., Bolan, N., Wang, H., & Tang, C. (2020). Chemical and biological immobilization mechanisms of potentially toxic elements in biochar amended soils. *Critical Reviews in Environmental Science and Technology, 50*, 903–978.

Basta, N., & Gradwohl, R. (2000). Estimation of Cd, Pb, and Zn bioavailability in smelter-contaminated soils by a sequential extraction procedure. *Journal of Soil Contamination, 9*, 149–164.

Beesley, L., Moreno-Jiménez, E., & Gomez-Eyles, J. L. (2010). Effects of biochar and greenwaste compost amendments on mobility, bioavailability and toxicity of inorganic and organic contaminants in a multi-element polluted soil. *Environmental Pollution, 158*, 2282–2287.

Beesley, L., Inneh, O. S., Norton, G. J., Moreno-Jimenez, E., Pardo, T., Clemente, R., & Dowson, J. J. (2014). Assessing the influence of compost and biochar amendments on the mobility and toxicity of metals and arsenic in a naturally contaminated mine soil. *Environmental Pollution, 186*, 195–202.

Brian, R., Joseph, S., Cui, L., Pan, G., Li, L., Liu, X., Zhang, A., Rutlidge, H., Wong, S., Chia, C., Marjo, C., Gong, B., Munroe, P., & Donne, S. (2014). A three-year experiment confirms continuous immobilization of cadmium and lead in contaminated paddy-field with biochar amendment. *Journal of Hazardous Materials, 272*, 121–128.

Castaldi, P., Melis, P., Silvetti, M., Deiana, P., & Garau, G. (2009). Influence of pea and wheat growth on Pb, Cd, and Zn mobility and soil biological status in a polluted amended soil. *Geoderma, 151*, 241–248.

Chen, D., Liu, X., Bian, R., Cheng, K., Zhang, X., Zheng, J., Joseph, S., Crowley, D., Pan, G., & Li, L. (2018). Effects of biochar on availability and plant uptake of heavy metals – A meta analysis. *Journal of Environmental Management, 222*, 76–85.

Dal Corso, G. (2012). Heavy metal toxicity in plants. In *Plants and Heavy Metals, Springer Briefs in Molecular Science*. Springer (pp. 1–25). Dordrecht, Netherlands.

Diquattro, S., Garau, G., Lauro, G. P., Silvetti, M., Deiana, S., & Castaldi, P. (2018). Municipal solid waste compost as a novel sorbent for antimony(V): Adsorption and release trials at acidic pH. *Environmental Science and Pollution Research, 25*, 5603–5615.

Evangelou, M. W., Fellet, G., Ji, R., & Schulin, R. (2015). Phytoremediation and biochar application as an amendment. In A. A. Ansari, S. S. Gill, R. Gill, G. R. Lanza, & L. Newman (Eds.), *Phytoremediation, Springer International Publishing* (pp. 253–263). Netherlands.

Ford, R. G., Wilkin, R. T., & Puls, R. W. (2007). Monitored natural attenuation of inorganic contaminants in ground water Volume 2 – Assessment for non-radionuclides including arsenic, cadmium, chromium, copper, lead, nickel, nitrate, perchlorate, and selenium. EPA Report number: EPA/600/R-07/140.

Garau, G., Mele, E., Castaldi, P., Lauro, G. P., & Deiana, S. (2015). Role of poligalacturonic acid and the cooperative effect of caffeic and maleic acids on the toxicity of

Cu(II) towards triticale plants ((× Triticosecale Wittm). *Biology and Fertility of Soils, 51*, 535–544.

Garau, G., Diquattro, S., Lauro, G. P., Deiana, S., & Castaldi, P. (2019a). Influence of Pb(II) in the sorption of As(V) by a Ca-polygalacturonate network, a root mucilage model. *Soil Science and Plant Nutrition, 65*, 305–315.

Garau, G., Lauro, G. P., Diquattro, S., Garau, M., & Castaldi, P. (2019b). Sb(V) adsorption and desorption onto ferrihydrite: Influence of pH and competing organic and inorganic anions. *Environmental Science and Pollution Research, 26*, 27268–27280.

Garau, G., Roggero, P. P., Diquattro, S., Garau, M., Pinna, M. V., & Castaldi, P. (2021a). Innovative amendments derived from industrial and municipal wastes enhance plant growth and soil functions in PTE-polluted environments. *Italian Journal of Agronomy, 16*, 1777–1793.

Garau, M., Castaldi, P., Diquattro, S., Pinna, M. V., Senette, C., Roggero, P. P., & Garau, G. (2021b). Combining grass and legume species with compost for assisted phytostabilization of contaminated soils. *Environmental Technology & Innovation, 22*, 101387–101399.

Gazzetta Ufficiale (1992). Metodi Ufficiali di Analisi Chimica dei Suoli. DM 11 Maggio 1992, Suppl. G.U. 121, 25 Maggio 1992. [Official Gazette of the Italian Republic. Official Methods for Chemical Analysis of Soils. Ministerial Decree 05–25–1992].

He, E., Yang, Y., Xu, Z., Qiu, H., Yang, F., Peijnenburg, W. J. G. M., Zhang, W., Qiu, R., & Wang, S. (2019). Two years of aging influences the distribution and lability of metal(loid)s in a contaminated soil amended with different biochars. *Science of the Total Environment, 673*, 245–253.

Herath, I., Vithanage, M., & Bundschuh, J. (2017). Antimony as a global dilemma: Geochemistry, mobility, fate and transport. *Environmental Pollution, 223*, 545–559.

Ho, Y. S., & Mckay, G. (2000). The kinetics of sorption of divalent metal ions onto sphagnum moss peat. *Water Research, 34*, 735–742.

Ippolito, J. A., Strawn, D. G., Scheckel, K. G., Novak, J. M., Ahmedna, M., & Niandou, M. A. S. (2012). Macroscopic and molecular investigations on copper sorption by a steam-activated biochar. *Journal of Environmental Quality, 41*, 1150–1156.

Janu, R., Mrlik, V., Ribitsch, D., Hofman, J., Sedláček, P., Bielská, L., & Soja, G. (2021). Biochar surface functional groups as affected by biomass feedstock, biochar composition and pyrolysis temperature. *Carbon Resources Conversion, 4*, 36–46.

Kamran, M., Zafar Malik, Z., Parveen, A., Huang, L., Riaz, M., Bashir, S., Mustafa, A., Abbasi, G. H., Xue, B., & Ali, U. (2020). Ameliorative effects of biochar on Rapeseed (Brassica napus L.) growth and heavy metal immobilization in soil irrigated with untreated wastewater. *Journal of Plant Growth Regulation, 39*, 266–281.

Kuzyakov, Y., & Blagodatskaya, E. (2015). Microbial hotspots and hot moments in soil: Concept & review. *Soil Biology & Biochemistry, 83*, 184–199.

Liu, R., Liu, F., Hu, C., He, Z., Liu, H., & Qu, J. (2015). Simultaneous removal of Cd(II) and Sb(V) by Fe–Mn binary oxide: Positive effects of Cd(II) on Sb(V) adsorption. *Journal of Hazardous Materials, 300*, 847–854.

Maiti, S. K., & Ghosh, D. (2021). Use of biochar as an amendment for remediation of heavy metal-contaminated soils. In Majeti N. V. Prasad (Ed.), *Handbook of assisted and amendment: Enhanced Sustainable Remediation Technology* (pp 163–177).

Manzano, R., Diquattro, S., Roggero, P. P., Pinna, M. V., Garau, G., & Castaldi, P. (2020). Addition of softwood biochar to contaminated soils decreases the mobility, leachability and bioaccesibility of potentially toxic elements. *Science of the Total Environment, 739*, 139946–139957.

MIPAAF (2015). Aggiornamento degli allegati 2, 6 e 7 al decreto legislativo n. 75 del 29 aprile 2010. Riordino e revisione della disciplina in materia di fertilizzanti, a norma dell'articolo 13 della legge 7 luglio 2009, n. 88. Gazz Uff della Rep Ital Anno 156°.

Mohamed, B. A., Ellis, N., Soo Kim, C., & Bi, X. (2017). The role of tailored biochar in increasing plant growth, and reducing bioavailability, phytotoxicity, and uptake of heavy metals in contaminated soil. *Environmental Pollution, 230*, 329–338.

Mohapatra, D., Singh, P., Zhang, W., & Pullammanappallil, P. (2005). The effect of citrate, oxalate, acetate, silicate and phosphate on stability of synthetic arsenic-loaded ferrihydrite and Al-ferrihydrite. *Journal of Hazardous Materials, 124*, 95–100.

Mukome, F. N. D., Zhang, X., Silva, L. C. R., Six, J., & Parikh, S. J. (2013). Use of chemical and physical characteristics to investigate trends in biochar feedstocks. *Journal of Agricultural and Food Chemistry, 61*(9), 2196–2204.

Namgay, T., Singh, B., & Singh, B. P. (2010). Influence of biochar application to soil on the availability of As, Cd, Cu, Pb, and Zn to maize (Zea mays L.). *Australian Journal of Soil Research, 48*, 638–647.

Olsen, S. R. (1954). Estimation of available phosphorus in soils by extraction with sodium bicarbonate, USDA Circular 939. U.S. Gov. Print. Office, Washington, DC

Palansooriya, K. N., Shaheen, S. M., Chen, S. S., Tsang, D. C. W., Hashimoto, Y., Hou, D. Y., Bolan, N. S., Rinklebe, J., & Ok, Y. S. (2020). Soil amendments for immobilization of potentially toxic elements in contaminated soils: A critical review. *Environment International, 134*, 105046–105074.

Piga, G., Gonçalves, D., Thompson, T. J. U., Brunetti, A., Malgosa, A., & Enzo, S. (2016). Understanding the crystallinity indices behavior of burned bones and teeth by ATR-IR and XRD in the presence of bioapatite mixed with other phosphate and carbonate phases. *International Journal of Spectroscopy*, Article ID 4810149.

Pinna, M. V., Baronti, S., Miglietta, F., & Pusino, A. (2016). Photooxidation of foramsulfuron: Effects of char substances. *Journal of Photochemistry and Photobiology A, 326*, 16–20.

Pinna, M. V., Baronti, S., Liguori, F., & Pusino, A. (2020). Assessment of biochars obtained at two different pyrolysis temperatures to mitigate pollution due to Lumax. *Fresenius Environmental Bulletin, 29*, 4497–4504.

Robati, D. (2013). Pseudo-second-order kinetic equations for modeling adsorption systems for removal of lead ions using multi-walled carbon nanotube. *Journal of Nanostructure in Chemistry, 3*, 55.

Rodríguez-Vila, A., Selwyn-Smith, H., Enunwa, L., Smail, I., Covelo, E. F., & Sizmur, T. (2018). Predicting Cu and Zn sorption capacity of biochar from feedstock C/N ratio and pyrolysis temperature. *Environmental Science and Pollution Research, 25*, 7730–7739.

Santos, S., Costa, C. A. E., Duarte, A. C., Scherer, H. W., Schneider, R. J., Esteves, V. I., & Santos, E. B. H. (2010). Influence of different organic amendments on the potential availability of metals from soil: A study on metal fractionation and extraction kinetics by EDTA. *Chemosphere, 78*, 389–396.

Schnitzer, M., & Gupta, U. C. (1965). Determination of acidity in soil organic matter. *Soil Science Society of America Journal, 29*, 274–277.

Shen, Z., Zhang, Y., McMillan, O., O'Connor, D., & Hou, D. (2020). The use of biochar for sustainable treatment of contaminated soils. In D. Hou (Ed.) *Sustainable remediation of contaminated soil and groundwater. Materials, Processes, and Assessment (*pp 119–167).

Silverstein, R. M., Bassler, G. C., & Morrill, T. C. (1981). In John Wiley and Sons (Eds*.), Spectrometric identification of organic compounds* (4th ed., pp 112–115). New York.

Silvetti, M., Castaldi, P., Holm, P. E., Deiana, S., & Lombi, E. (2014). Leachability, bioaccessibility and plant availability of trace elements in contaminated soils treated with industrial byproducts and subjected to oxidative/reductive conditions. *Geoderma, 214–215*, 204–212.

Silvetti, M., Garau, G., Demurtas, D., Marceddu, S., Deiana, S., & Castaldi, P. (2017). Influence of lead in the sorption of arsenate by municipal solid waste composts: Metal(loid) retention, desorption and phytotoxicity. *Bioresource Technology, 225*, 90–98.

Sohi, S. P., Krull, E., Lopez-Capel, E., & Bol, R. (2010). A review of biochar and its use and function in soil. *Advances in Agronomy*, 1st ed. Elsevier Inc.

Soria, R. I., Rolfe, S. A., Pazmiño Betancourth, M., & Thornton, S. F. (2020). The relationship between properties of plant-based biochars and sorption of Cd(II), Pb(II) and Zn(II) in soil model systems. *Heliyon,* 6, e05388.

Stella Mary, G., Sugumaran, P., & Niveditha, S. (2016). Production, characterization and evaluation of biochar from pod (Pisum sativum), leaf (Brassica oleracea) and peel (Citrus sinensis) wastes. *International Journal of Recycling of Organic Waste in Agriculture, 5*, 43–53.

Takeda, A., Tsukada, H., Takaku, Y., & Hisamatsu, S. (2009). Fractionation of metal complexes with dissolved organic matter in a rhizosphere soil solution of a humus-rich andosol using size exclusion chromatography with inductively coupled plasma-mass spectrometry. *Soil Science and Plant Nutrition, 55*, 349–357.

Tella, M., & Pokrovski, G. S. (2012). Stability and structure of pentavalent antimony complexes with aqueous organic ligands. *Chemical Geology, 292–293*, 57–68.

Uchimiya, M., Chang, S., & Klasson, K. T. (2011). Screening biochars for heavy metal retention in soil: Role of oxygen functional groups. *Journal of Hazardous Materials, 190*, 432–441.

UNI EN 13040 (2008). European standard, soil improvers and growing media, sample preparation for chemical and physical tests, determination of dry matter content, moisture content and laboratory compacted bulk density.

Wang, S., Cai, L. M., Wen, H. H., Luo, J., Wang, Q. S., & Liu, X. (2019). Spatial distribution and source apportionment of heavy metals in soil from a typical county-level city of Guangdong Province, China. *Science of the Total Environment, 655*, 92–101.

Wilson, S. C., Lockwood, P. V., Ashley, P. M., & Tighe, M. (2010). The chemistry and behaviour of antimony in the soil environment with comparisons to arsenic: A critical review. *Environmental Pollution, 158*, 1169–1181.

Wu, H. X., Sun, P., Lu, S., Ren, L. X., & Chen, Y. Y. (2020). Enteromorpha prolifera biochar promoted the immobilization of Pb in soil and reduced the phytotoxicity of Pb to Vetiveriazizanioides (L.) Nash. *China Environmental Science, 40*, 3530–3538.

Xu, X., Zhao, Y., Sima, J., Zhao, L., Masek, O., & Cao, X. (2017). Indispensable role of biochar inherent mineral constituents in its environmental applications: A review. *Bioresource Technology, 241*, 887–899.

Zhang, F., Wang, X., Xionghui, J., & Ma, L. (2016). Efficient arsenate removal by magnetite-modified water hyacinth biochar. *Environmental Pollution, 216*, 575–583.

Zhao, L., Cao, X., Mašek, O., & Zimmerman, A. (2013). Heterogeneity of biochar properties as a function of feedstock sources and production temperatures. *Journal of Hazardous Materials, 256*, 1–9.